THE JOURNAL OF PHYSICAL CHEMISTRY LETTERS
A JOURNAL OF THE AMERICAN CHEMICAL SOCIETY

pubs.acs.org/JPCL

Letter

Retrained Generic Antibodies Can Recognize SARS-CoV-2

Yanxiao Han, Katherine D. McReynolds, and Petr Král*

Cite This: J. Phys. Chem. Lett. 2021, 12, 1438−1442

Read Online

ACCESS | Metrics & More | Article Recommendations | Supporting Information

ABSTRACT: The dramatic impact novel viruses can have on humans could be more quickly mitigated if generic antibodies already present in one's system are temporarily retrained to recognize these viruses. This type of intervention can be administered during the early stages of infection, while a specific immune response is being developed. With this idea in mind, double-faced peptide-based boosters were computationally designed to allow recognition of SARS-CoV-2 by Hepatitis B antibodies. One booster face is made of ACE2-mimic peptides that can bind to the receptor binding domain (RBD) of SARS-CoV-2. The other booster face is composed of a Hepatitis B core-antigen, targeting the Hepatitis B antibody fragment. Molecular dynamics simulations revealed that the designed boosters have a highly specific and stable binding to both the RBD and the antibody fragment (AF). This approach can provide a cheap and efficient neutralization of emerging pathogens.

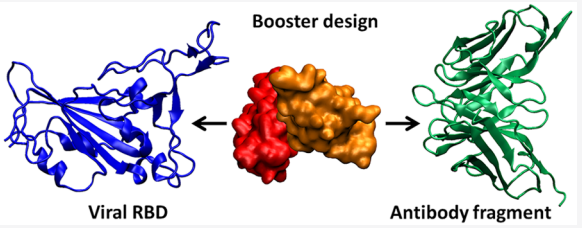

In the last several decades, zoonotic viral pathogens (SARS, MERS, Dengue, Ebola, Zika, H1N1, etc.) have become a major global public heath problem due to their rapid spread within the highly concentrated and mobile human population.[1] Fortunately, none of the above related diseases have reached a truly global scale due to the highly organized actions taken to stop their spread, sometimes in combination with large local fatalities. However, SARS-CoV-2 took the world by surprise with its very rapid spread and moderate mortality. It has caused a devastating COVID-19 pandemic with large numbers of fatalities and wide-ranging socioeconomic disruptions.

COVID-19 has been addressed on many parallel fronts, including the development of antiviral drugs,[2−7] antibody therapies,[8,9] and vaccines.[10,11] Ultimately, to become protected, humans can gain antibodies through convalescent plasma therapies, vaccinations,[12] or real infections. However, these approaches have various limitations. The preparation of antibodies is a complex process, and their delivery is instantaneous; however, such antibodies have shorter lifetimes. Vaccinations need to be repeated, it takes some time before the antibody response is robust and effective, and the vaccines might not be effective for everybody. Finally, the actual viral infections can have large consequences.

To address novel viral infections in an emergency mode, we propose an alternative approach to quickly redirect (train) the immune response. In particular, we show that one can design interfacial molecular boosters that allow generic antibodies preexisting in the human body to recognize novel viruses, thereby allowing their selective clearance by standard pathways.[13] Such double-faced boosters can provide highly specific binding of generic antibodies (resulting from vaccination against other diseases) with novel viruses. Hepatitis B antibodies are a good choice for recognizing new viruses, due to their long lifetimes (30 years).[14] As a practical example of this treatment, we designed and simulated boosters composed of the ACE2-based peptide inhibitors that bind to the Spike receptor binding domain (RBD) of SARS-CoV-2, and segments of the Hepatitis B antigen, which bind to the Hepatitis B antibodies. This computational study could provide guidance in the preparation of active therapeutics against emerging pathogens with the combined advantages of small-protein and antibody therapies. However, the designed boosters should be thoroughly tested and further optimized in follow-up experimental/computational studies.

Booster Design. Each booster has two connected and outside oriented faces, including the ACE2-mimic (Face 1, red) and the antigen of Hepatitis B (Face 2, orange), as shown in Figure 1a−c. Face 1 is formed by peptide inhibitors of SARS-CoV-2, very similar to those designed in our previous work.[2] Their components, such as α-helices and the β-hairpin segment, were extracted from ACE2 that was in close contact with the RBD of SARS-CoV-2. Face 2 is a region extracted from the Hepatitis B core-antigen that is recognized by the Hepatitis B antibodies.

Booster 1: Face 1 is composed of the $\alpha_1\alpha_2$ helices of ACE2 (19−102 amino acids), which are in close contact with the RBD of SARS-CoV-2. Face 2 is the Hepatitis B core-antigen without the 66−91 amino acids. Because these amino acids form a flexible random coil, they are excluded in Booster 1 to make a stable structure. The two faces are connected by a

Received: December 8, 2020
Accepted: January 21, 2021

https://dx.doi.org/10.1021/acs.jpclett.0c03615
J. Phys. Chem. Lett. 2021, 12, 1438−1442

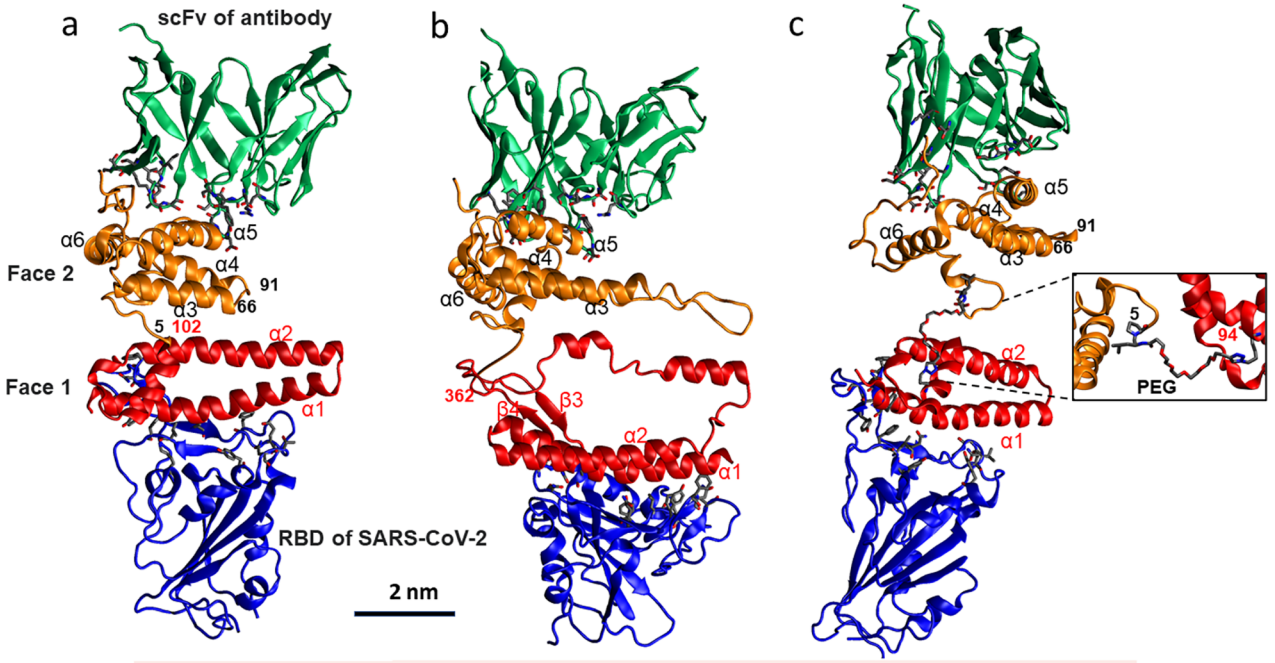

d

Residue	34	94	95	96	155	156	157	158	159	180	181	182	183
	R	D	T	S	I	D	L	S	S	Y	G	G	S
	184	186	198	199	200	201	207	226	228	229	230	231	
	I	Y	S	K	T	S	K	S	G	D	G	Y	

e

Residue	417	446	449	453	455	456	473	475	476	486	487	489	493	496	498	500	501	502	505
	K	G	Y	Y	L	F	Y	A	G	F	N	Y	Q	G	Q	T	N	G	Y

Figure 1. Structure of double-faced boosters bound to the Spike RBD and the AF (scFv). (a) Booster 1 is composed of Face 1 formed by the ACE2-mimic (19−102 amino acids[15]) and Face 2 formed by the Hepatitis B antigen (without 66−91 residues[16]). (b) Booster 2 has inhibitor **3** from ref 2 as Face 1 and the Hepatitis B antigen[16] as Face 2. (c) Booster 3 has the same faces as Booster 1 but with a PEG linker in between (inset). (d) Amino acids of the AF that initially interact with Face 2. (e) Amino acids of the RBD that initially interact with Face 1. Color scale: green, antibody; orange, antigen (Face 2); red, ACE2-mimic (Face 1); blue, RBD of SARS-CoV-2; gray, C atom; red, O atom; blue, N atom. ACE2: angiotensin-converting enzyme 2, the cellular receptor of SARS-CoV-2.

peptide bond formed between the 102nd amino acid of the ACE2 helices and the fifth amino acid of the Hepatitis B core-antigen, as shown in Figure 1a.

Booster 2: Face 1 is the previously designed SARS-CoV-2 Inhibitor 3.[2] Face 2 contains the 5−145 amino acids of the Hepatitis B core-antigen. The two faces are linked by a peptide bond formed between the 362nd amino acid of Inhibitor 3 and the fifth amino acid of the Hepatitis B core-antigen (Figure 1b).

Booster 3: Both faces have the same components as Booster 1 but with a polyethylene glycol (PEG) linker between the 94th amino acid of the ACE2 helices and the fifth amino acid of the Hepatitis B core-antigen, as shown in the inset of Figure 1c. A highly biocompatible PEG chain adds a nonpeptide linkage between the faces, which may maximize the conformational integrity of individual faces. Figure S1 shows the detailed ChemDraw structure of the PEG linkage in Booster 3.

As shown in Figure 1a−c, the boosters were initially placed with Face 1 (red) binding to the RBD of SARS-CoV-2 (blue) and Face 2 (orange) binding to the antibody fragment (AF) (green), the single-chain variable fragment (scFv) of the Hepatitis B antibody. The initial binding configurations were based on the 6LZG[15] and 6CWD[16] PDB crystal structures, respectively. The amino acids of the AF and the RBD that had initial contacts with the boosters (within 3 Å of boosters) are shown in licorice form in Figure 1a−c and are listed as IDs and names in Figure 1d,e, respectively.

Binding Conformations. Figure 2 displays the three-booster systems after 100 ns of simulations. The systems show some similarities but also remarkable differences. To better analyze the observations, we tracked the amino acids in the RBD and the AF, which are in close contact with the faces of boosters over the last 50 ns (500 frames) of the trajectories. We counted contact frames for amino acids where they are within 3 Å of their targets (Face 1 or Face 2). Figures S2−S4 show the number of contact frames of the RBD and the AF amino acids that are highly involved in the interactions with the three boosters. In Table S1, we list those hot spots (amino acids) in the RBD and the AF that have more than 250 contact frames out of 500 frames (last 50 ns). Most of these amino acids are polar. Because the Face 1 designs are ACE2-mimics, they bind to RBD in almost the same manner as ACE2.[17] Analogously, the Face 2 designs, based on the Hepatitis B core-antigen, should bind to the AF.

In Figure 2a, Booster 1 reveals that the two faces stay tightly bound with both the RBD and the AF, while at the same time the peptide structure remains largely preserved (insets). The RBD hot spots in binding with Face 1 are formed by 16 amino acids, including two new contacts marked in red (Table S1). The AF hot spots in binding with Face 2 are formed by 14 amino acids, where half of them are new binding contacts.

https://dx.doi.org/10.1021/acs.jpclett.0c03615
J. Phys. Chem. Lett. 2021, 12, 1438−1442

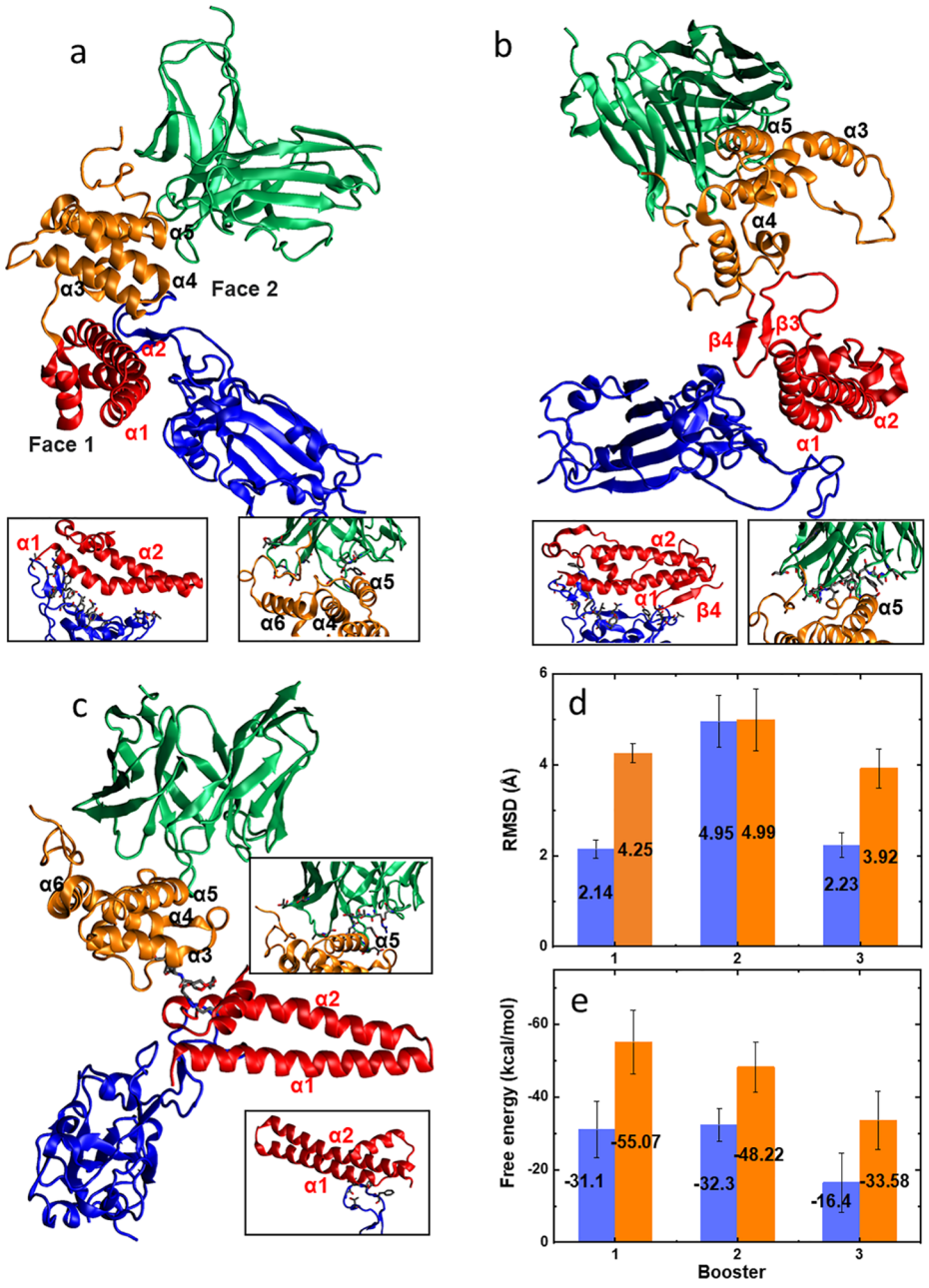

Figure 2. Simulated booster, RBD, and AF complexes. (a–c) Final conformations of Booster 1–3 systems at 100 ns. (d) Averaged RMSD for Face 1 (ACE2-mimic, blue bar) and Face 2 (antigen, orange bar). (e) Averaged free energy of binding of the RBD with Face 1 (blue bar) and antibody with Face 2 (orange bar).

Here the new binding contacts refer to amino acids that are not listed in the initially binding sets of amino acids, as shown in Figure 1d,e.

In Figure 2b, Booster 2 shows that the conformations of the α helices and the β hairpin remain largely intact during their binding with the RBD. Although Face 1 has an extra hairpin and coil structure, compared with Booster 1, it has the same number of hot spots, with no new contacts forming. The hot spots on the AF are formed by 19 amino acids, with one new contact (202T), which is less than the initial contact number shown in Figure 1d. Although Booster 2 has the longest sequence, it does not generate more contacts in the interface of the RBD and Face 1.

In Figure 2c, Booster 3 shows that Face 1 will likely dissociate from the RBD because only 6 hot spots remain bound, but Face 2 still binds to the AF with 14 amino acid hot spots. These results reveal that when the faces are attached by a long chain with the connecting points close to the sides of faces, the multivalent binding of the faces to their targets can be released by a fluctuative pulling generated by the linker, analogous to unzipping a double-stranded DNA from its ends. In contrast, if the same pulling was applied on the whole face or at least several of its regions, then it would be difficult to disturb the multivalent binding between the faces and their targets. In Boosters 1 and 2, the faces connected by a short peptide bond also develop other bindings within faces, so they behave like a rigid body, which can preserve the multivalency in binding with the RBD or the AF. In principle, one could preserve the multivalent binding in Booster 3 by joining its

https://dx.doi.org/10.1021/acs.jpclett.0c03615
J. Phys. Chem. Lett. 2021, 12, 1438–1442

faces with multiple PEG chains, or through having the attaching points at the centers of their faces.

Root-Mean-Square Deviations and Free Energies of Binding. To further quantify the booster-target binding, we calculated for each booster the root-mean-square deviation (RMSD) and the free energy of binding, $\Delta G_{\mathrm{MMGB-SA}}$. Figure S5 shows the time-dependent RMSDs of individual faces and whole boosters. The RMSDs of all three Boosters are large compared with their faces, revealing a relatively small rigidity of these Boosters. Moreover, Booster 3 has large RMSD fluctuations, which eventually become responsible for its unbinding in Face 1. Figure 2d shows the average RMSDs for the two faces obtained in the last 50 ns of simulations. Similar faces present in Boosters 1 and 3 have similar RMSDs, revealing that the instability of Booster 3 does not originate in Face 1 but in its PEG linker. Booster 2 with a somewhat different (larger) Face 1 shows a larger RMSD for Face 1, but this does not destabilize its binding. Overall, the RMSD values reflect the complexity of the involved faces.

Figure 2e shows $\Delta G_{\mathrm{MMGB-SA}}$ calculated for each face coupled to its target. Booster 1 has the strongest overall binding with the RBD and the AF, whereas Booster 3 has the weakest binding in both faces, where Face 1 of Booster 3 tends to dissociate from the RBD. Booster 2 has a free energy of binding (stability) positioned somewhere between Boosters 1 and 3.

To better understand the booster−target binding, the interaction energies (enthalpies) of binding components were separately calculated over the last 50 ns of simulations (Figures S6−S8) and separated into Coulombic and van der Waals (vdW) contributions. The interaction energies were calculated by the NAMD Energy plugin in VMD,[18] where the dielectric constant was set to 1. The large electrostatic binding energy contributions in all systems could be somewhat scaled down to reflect on the presence of water around the binding regions. However, the interaction energies again reveal a relatively stable binding of Boosters 1 and 2, as compared with Booster 3, which is in line with the free-energy calculations.

In summary, using classical MD simulations, we have shown that double-faced boosters provide highly promising pathways for targeting novel viruses by generic antibodies, in particular, SARS-CoV-2, by the Hepatitis B antibody. By allowing the immune system to recognize new viruses through utilizing antibodies preexisting in the organisms, one can establish new generic therapeutic methods. This method could be used in the rapid treatment of emerging pathogens.

MD Simulations. The two faces of boosters were separately bound to the RBD and the AF. All structures were directly based on the crystal structure of the human ACE2 protein bound to the RBD of SARS-CoV-2 (PDB ID: 6LZG)[15] and the Hepatitis B antigen bound to the AF.[16] Snapshots were taken by VMD.[18]

The systems were simulated using NAMD2,[19] the CHARMM36 protein force field[20] and the CHARMM36 general force field. The simulations were conducted with the Langevin dynamics ($\gamma_{\mathrm{Lang}} = 1\ \mathrm{ps}^{-1}$) in the NpT ensemble at temperature of $T = 310$ K and pressure of $p = 1$ bar. The particle-mesh Ewald (PME) method was used to evaluate a long-range Coulombic coupling, with periodic boundary conditions applied.[21] The time step was set to 2 fs. The long-range van der Waals and Coulombic coupling were evaluated every one and two time steps, respectively. After 2000 steps of minimization, the solvent molecules were equilibrated for 3 ns, whereas the complexes were restrained using harmonic forces with a spring constant of 1 kcal/(mol Å). Next, the systems were equilibrated in 100 ns production MD runs with restraints on the top part of the AF. All systems were simulated in 150 mM NaCl solutions with the TIP3P water model.[22]

RMSD Calculations. The time-dependent RMSDs for Face 1 and Face 2 (Figure S4) were calculated from

$$\mathrm{RMSD}_{\alpha}(t_j) = \sqrt{\frac{\sum_{\alpha=1}^{N_\alpha} (\vec{r}_\alpha(t_j) - \vec{r}_\alpha(t_0))^2}{N_\alpha}} \quad (1)$$

where N_α is the number of atoms whose positions are being compared, $\vec{r}_\alpha(t_j)$ is the position of atom α at time t_j, and $\vec{r}_\alpha(t_0)$ is the initial coordinate. The selection of coordinates contains all of the atoms in Face 1 or Face 2, excluding hydrogens. The time-dependent RMSD was averaged over the last 50 ns of simulation time, which corresponds to the last 500 frames of each trajectory, as shown in Figure 2d. The standard deviations are shown by the error bars.

MMGB-SA Calculations. We used the molecular mechanics generalized Born−surface area (MMGB-SA) method[23,24] to estimate the relative binding free energies between booster faces and their binders (RBD or AF). The free energies were estimated from separate MMGB-SA calculations for three systems related to the face and its binder (the face, the binder of the face, and the complex of the face and its binder) in configurations extracted from the MD trajectories of the whole complex in the explicit solvent. The MMGB-SA free energies of the extracted configurations of the three systems were calculated as

$$G_{\mathrm{tot}} = E_{\mathrm{MM}} + G_{\mathrm{solv-p}} + G_{\mathrm{solv-np}} - T\Delta S_{\mathrm{conf}}$$

where E_{MM}, $G_{\mathrm{solv-p}}$, $G_{\mathrm{solv-np}}$, and ΔS_{conf} are the sum of bonded and Lennard-Jones energy terms, the polar contribution to the solvation energy, the nonpolar contribution, and the conformational entropy, respectively. The E_{MM}, $G_{\mathrm{solv-p}}$, and $G_{\mathrm{solv-np}}$ terms were calculated using the NAMD 2 package[19] generalized Born implicit solvent model,[25] with a solvent dielectric constant of $\varepsilon = 78.5$. The $G_{\mathrm{solv-np}}$ term for each system configuration was calculated in NAMD as a linear function of the solvent-accessible surface area (SASA), determined using a probe radius of 1.4 Å, as $G_{\mathrm{solv-np}} = \mathrm{SASA}\ \gamma$, where $\gamma = 0.00542$ kcal/(mol Å^2) is the surface tension. The ΔS_{conf} term was neglected, as the entropy term is often calculated with a large computational cost and low prediction accuracy, which is likely to be similar for the studied systems, which differ in the connecting part of the two faces.[26,27] Because the G_{tot} values are obtained for configurations extracted from the trajectories of complexes, G_{tot} does not include the free energies of the face reorganization; the correct free energies of binding should consider the configurations of separately relaxed systems. The approximate binding free energies of the studied complexes were calculated as $\langle \Delta G_{\mathrm{MMGB-SA}} \rangle = \langle G_{\mathrm{tot}}(\text{face-binder}) - G_{\mathrm{tot}}(\text{face}) - G_{\mathrm{tot}}(\text{binder}) \rangle$, where face-binder represents the complex of face with its binder, and the $\langle$averaging$\rangle$ is performed over configurations within the second half of the calculated trajectories.

■ ASSOCIATED CONTENT

Supporting Information

The Supporting Information is available free of charge at https://pubs.acs.org/doi/10.1021/acs.jpclett.0c03615.

https://dx.doi.org/10.1021/acs.jpclett.0c03615
J. Phys. Chem. Lett. 2021, 12, 1438−1442

Figure S1. ChemDraw structures for linker design of Booster 3. Figure S2. Booster 1 system. Figure S3. Booster 2 system. Figure S4. Booster 3 system. Figure S5. RMSD of the components in the three booster systems. Figure S6. Interaction energy between each face and its target in Booster 1. Figure S7. Interaction energy between each face and its target in Booster 2. Figure S8. Interaction energy between each face and its target in Booster 3. Table S1. Amino acids with more than 250 contact times in Figures S2−S4 .(PDF)

AUTHOR INFORMATION

Corresponding Author

Petr Král − *Department of Chemistry, University of Illinois at Chicago, Chicago, Illinois 60607, United States; Departments of Physics, Pharmaceutical Sciences, and Chemical Engineering, University of Illinois at Chicago, Chicago, Illinois 60607, United States;* orcid.org/0000-0003-2992-9027; Email: pkral@uic.edu

Authors

Yanxiao Han − *Department of Chemistry, University of Illinois at Chicago, Chicago, Illinois 60607, United States;* orcid.org/0000-0002-1684-6073

Katherine D. McReynolds − *Department of Chemistry, California State University, Sacramento, Sacramento, California 95819-6057, United States;* orcid.org/0000-0001-8395-3066

Complete contact information is available at: https://pubs.acs.org/10.1021/acs.jpclett.0c03615

Notes

The authors declare no competing financial interest.

ACKNOWLEDGMENTS

P.K. and Y.H. gratefully acknowledge the funding obtained from the UIC Center for Clinical and Translational Science. K.D.M. acknowledges the funding obtained from NIH-NIGMS 5SC3GM119521.

REFERENCES

(1) Belay, E. D.; Kile, J. C.; Hall, A. J.; Barton-Behravesh, C.; Parsons, M. B.; Salyer, S.; Walke, H. Zoonotic Disease Programs for Enhancing Global Health Security. *Emerging Infect. Dis.* **2017**, *23*, S65−S70.

(2) Han, Y.; Král, P. Computational Design of ACE2-Based Peptide Inhibitors of SARS-CoV-2. *ACS Nano* **2020**, *14*, 5143−5147.

(3) Chaturvedi, P.; Han, Y.; Král, P.; Vukovic, L. Adaptive Evolution of Peptide Inhibitors for Mutating SARS-CoV-2. *Adv. Theory and Simul* **2020**, *3*, 2000156.

(4) Cao, L.; Goreshnik, I.; Coventry, B.; Case, J. B.; Miller, L.; Kozodoy, L.; Chen, R. E.; Carter, L.; Walls, A. C.; Park, Y.-J.; Strauch, E.-M.; Stewart, L.; Diamond, M. S.; Veesler, D.; Baker, D. De Novo Design of Picomolar SARS-CoV-2 miniprotein Inhibitors. *Science* **2020**, *370*, 426−431.

(5) Yoo, J. H. Uncertainty about the Efficacy of Remdesivir on COVID-19. *J. Korean Med. Sci.* **2020**, *35*, No. e221.

(6) Wu, R.; Wang, L.; Kuo, H. D.; Shannar, A.; Peter, R.; Chou, P. J.; Li, S.; Hudlikar, R.; Liu, X.; Liu, Z.; Poiani, G. J.; Amorosa, L.; Brunetti, L.; Kong, A. N. An Update on Current Therapeutic Drugs Treating COVID-19. *Curr. Pharmacol. Rep.* **2020**, *6*, 56−70.

(7) Wu, C.; Liu, Y.; Yang, Y.; Zhang, P.; Zhong, W.; Wang, Y.; Wang, Q.; Xu, Y.; Li, M.; Li, X.; Zheng, M.; Chen, L.; Li, H. Analysis of Therapeutic Targets for SARS-CoV-2 and Discovery of Potential Drugs by Computational Methods. *Acta Pharm. Sin. B* **2020**, *10*, 766−788.

(8) Jahanshahlu, L.; Rezaei, N. Monoclonal Antibody as a Potential Anti-COVID-19. *Biomed. Pharmacother.* **2020**, *129*, 110337.

(9) Ledford, H. Coronavirus: Will the World Benefit From Antibody Therapies? *Nature* **2020**, *584*, 333.

(10) Ali, I.; Alharbi, O. M. L. COVID-19: Disease, Management, Treatment, and Social Impact. *Sci. Total Environ.* **2020**, *728*, 138861.

(11) Jeyanathan, M.; Afkhami, S.; Smaill, F.; Miller, M. S.; Lichty, B. D.; Xing, Z. Immunological Considerations for COVID-19 Vaccine Strategies. *Nat. Rev. Immunol.* **2020**, *20*, 615−632.

(12) Humphrey, J. H. Antibodies-Structure and Biological Function. *Proc. R. Soc. Med.* **1967**, *60*, 591−594.

(13) Han, Y.; McReynolds, K.; Král, P. Retrained Generic Antibodies Can Recognize SARS-CoV-2. *ChemRxiv* **2020**, DOI: 10.26434/chemrxiv.13249559.v1.

(14) Van Damme, P.; Dionne, M.; Leroux-Roels, G.; Van Der Meeren, O.; Di Paolo, E.; Salaun, B.; Surya Kiran, P.; Folschweiller, N. Persistence of HBsAg-Specific Antibodies and Immune Memory Two to Three Decades after Hepatitis B Vaccination in Adults. *J. Viral. Hepat.* **2019**, *26*, 1066−1075.

(15) Wang, Q.; Zhang, Y.; Wu, L.; Niu, S.; Song, C.; Zhang, Z.; Lu, G.; Qiao, C.; Hu, Y.; Yuen, K.-Y.; Wang, Q.; Zhou, H.; Yan, J.; Qi, J. Structural and Functional Basis of SARS-CoV-2 Entry by Using Human ACE2. *Cell* **2020**, *181*, 894−904.e9.

(16) Eren, E.; Watts, N. R.; Dearborn, A. D.; Palmer, I. W.; Kaufman, J. D.; Steven, A. C.; Wingfield, P. T. Structures of Hepatitis B Virus Core- and e-Antigen Immune Complexes Suggest Multi-Point Inhibition. *Structure* **2018**, *26*, 1314−1326.

(17) Amin, M.; Sorour, M. K.; Kasry, A. Comparing the Binding Interactions in the Receptor Binding Domains of SARS-CoV-2 and SARS-CoV. *J. Phys. Chem. Lett.* **2020**, *11*, 4897−4900.

(18) Humphrey, W.; Dalke, A.; Schulten, K. VMD: Visual Molecular Dynamics. *J. Mol. Graphics* **1996**, *14*, 33−38.

(19) Phillips, J. C.; Braun, R.; Wang, W.; Gumbart, J.; Tajkhorshid, E.; Villa, E.; Chipot, C.; Skeel, R. D.; Kalé, L.; Schulten, K. Scalable Molecular Dynamics with NAMD. *J. Comput. Chem.* **2005**, *26*, 1781−1802.

(20) MacKerell, A. D.; et al. All-Atom Empirical Potential for Molecular Modeling and Dynamics Studies of Proteins. *J. Phys. Chem. B* **1998**, *102*, 3586−3616.

(21) Darden, T.; York, D.; Pedersen, L. Particle Mesh Ewald: An N log(N) Method for Ewald Sums in Large Systems. *J. Chem. Phys.* **1993**, *98*, 10089−10092.

(22) Boonstra, S.; Onck, P. R.; van der Giessen, E. CHARMM TIP3P Water Model Suppresses Peptide Folding by Solvating the Unfolded State. *J. Phys. Chem. B* **2016**, *120*, 3692−3698.

(23) Homeyer, N.; Gohlke, H. Free Energy Calculations by the Molecular Mechanics Poisson-Boltzmann Surface Area Method. *Mol. Inf.* **2012**, *31*, 114−122.

(24) Vergara-Jaque, A.; Comer, J.; Monsalve, L.; González-Nilo, F. D.; Sandoval, C. Computationally Efficient Methodology for Atomic-Level Characterization of Dendrimer-Drug Complexes: A Comparison of Amine- and Acetyl-Terminated PAMAM. *J. Phys. Chem. B* **2013**, *117*, 6801−6813.

(25) Tanner, D. E.; Chan, K.-Y.; Phillips, J. C.; Schulten, K. Parallel Generalized Born Implicit Solvent Calculations with NAMD. *J. Chem. Theory Comput.* **2011**, *7*, 3635−3642.

(26) Abroshan, H.; Akbarzadeh, H.; Parsafar, G. A. Molecular Dynamics Simulation and MM-PBSA Calculations of Sickle Cell Hemoglobin in Dimer form with Val, Trp, or Phe at the Lateral Contact. *J. Phys. Org. Chem.* **2010**, *23*, 866−877.

(27) Massova, I.; Kollman, P. A. Computational Alanine Scanning To Probe Protein-Protein Interactions: A Novel Approach To Evaluate Binding Free Energies. *J. Am. Chem. Soc.* **1999**, *121*, 8133−8143.